CHALMERS
UNIVERSITY OF TECHNOLOGY

Structural Investigation of Alkali-Activated Blast Furnace Slag

Influence of Water Glass Modulus on Reaction Kinetics, Microstructure and Mechanical Properties

Master's thesis in Materials Chemistry

EINAR SAHLE

DEPARTMENT CHEMISTRY AND CHEMICAL ENGINEERING
CHALMERS UNIVERSITY OF TECHNOLOGY
Gothenburg, Sweden 2026
www.chalmers.se

Master's thesis 2026

Structural Investigation of Alkali-Activated Blast Furnace Slag

Influence of Water Glass Modulus on Reaction Kinetics, Microstructure and Mechanical Properties

EINAR SAHLE

CHALMERS
UNIVERSITY OF TECHNOLOGY

Department of Chemistry and Chemical Engineering
Division of Applied Chemistry
Chalmers University of Technology
Gothenburg, Sweden 2026

Structural Investigation of Alkali-Activated Blast Furnace Slag
Influence of Water Glass Modulus on Reaction Kinetics, Microstructure and Mechanical Properties
EINAR SAHLE

Supervisor: Jenny Bengtsson and Emmanouela Leventaki, Chemistry and Chemical Engineering
Examiner: Diana Bernin, Chemistry and Chemical Engineering

Master's Thesis 2026
Department of Chemistry and Chemical Engineering
Division of Applied Chemistry
Chalmers University of Technology
SE-412 96 Gothenburg
Telephone +46 31 772 1000

Cover: Alkali-activated blast furnace slag used for Vicat needle test.

Typeset in LaTeX
Printed by Chalmers Reproservice
Gothenburg, Sweden 2026

Structural Investigation of Alkali-Activated Blast Furnace Slag
Influence of Water Glass Modulus on Reaction Kinetics, Microstructure and Mechanical Properties
EINAR SAHLE
Department of Chemistry and Chemical Engineering
Chalmers University of Technology

Abstract

Concrete production is associated with significant carbon dioxide emissions, primarily due to the the production of Ordinary Portland Cement (OPC), acting as the binder in conventional concrete. Alkali-activated materials (AAMs) have emerged as a promising alternative binder system with the potential to reduce the environmental impact of the construction industry. In alkali-activated systems, the chemistry and performance of the material are strongly influenced by the composition of the activator solution, particularly SiO_2/Na_2O ratio, also known as the water glass modulus.

This thesis investigates the influence of water glass modulus on the reaction behavior, microstructure development, and mechanical properties of alkali-activated blast furnace slag systems. Samples were prepared using ground granulated blast furnace slag (GGBS) with alkali activator solutions of varying water glass moduli. The materials were characterized in terms of setting time, chemical composition, reaction kinetics, microstructure and mechanical properties.

The results showed that the water glass modulus significantly affected setting time, porosity, structural development, and compressive strength. Modulus 1.0 exhibited the fastest structural development, highest compressive strength, and lowest surface area whilst still having an acceptable initial setting time (IST).

This study demonstrates the importance of optimizing sodium silicate modulus in AAMs systems and contributes to the understanding of how activator chemistry governs reaction mechanisms and material performance in sustainable cementitious binders.

Keywords: Alkali-activated materials, blast furnace slag, C-(A)-S-H, compressive strength, gel formation, isothermal calorimetry, reaction kinetics, Vicat, water glass modulus.

Acknowledgements

I would like to express my gratitude to my supervisors, Jenny and Emmanouela, for their guidance, support, and valuable feedback throughout this project. Their knowledge and encouragement have been greatly appreciated during the course of this project.

I would also like to thank Helen for her guidance and expertise within this research area, which contributed significantly to the project.

Thanks are also extended to Bruno for his assistance with laboratory equipment and practical support in the Architecture laboratories at Chalmers.

Finally, I would like to thank Diana for giving me the opportunity to be part of the research group and for providing a welcoming and inspiring research environment.

Einar Sahle, Gothenburg, June 2026

List of Acronyms

Below is the list of acronyms that have been used throughout this thesis listed in alphabetical order:

AAMs	Alkali-Activated Materials
BFS	Blast Furnace Slag
C-(A)-S-H	Calcium-alumino-silicate-hydrate
DTG	Derivative Thermogravimetry
EDS	Energy Dispersive X-ray Spectroscopy
FTIR	Fourier Transform Infrared Spectroscopy
GBFS	Granulated Blast Furnace Slag
GGBS	Ground Granulated Blast Furnace Slag
IST	Initial Setting Time
OPC	Ordinary Portland Cement
SEM	Scanning Electron Microscopy
TGA	Thermogravimetric Analysis

Contents

List of Figures

List of Tables

1
Introduction

Concrete is the secondly most used material in the world. Only water is used more and it is estimated that 8% of the global CO_2 emissions come from the concrete industry. Therefore finding alternatives to conventional concrete is of great interest for research [1]. Concrete is a composite material made up of an activator, binder, aggregates and additives. The activator is what initiates the chemical reaction of the binder, which then forms a hardened matrix that holds the system together. Aggregates, such as sand and gravel, provide the majority of the volume and contribute to the mechanical strength and dimensional stability of the material. Additives may be incorporated to modify properties such as workability, setting behavior, and durability. For conventional concrete Ordinary Portland Cement (OPC) is the main binder and a major source for CO_2 emissions [2].

One alternative to conventional concrete that has been explored in research is the use of alkali-activated materials (AAMs). In these materials OPC is replaced by industrial by-products as the main binder. Alkaline solutions containing sodium silicate (water glass) can be used as activators of low CO_2 footprint cementitious materials. The SiO_2/Na_2O ratio, also known as water glass modulus, governs the balance between available reactive species and dissolution [3].

AAMs are produced through the reaction of aluminosilicate binder precursor and an alkaline activator solution. There are different types of binder materials that can be used but some common ones include fly ash, blast furnace slag (BFS) and metakaolin. The binder of AAMs is what make the material attractive from a sustainability perspective. During activation, the alkaline solution dissolves reactive silica and alumina species from the binder precursor. This then rearranges and polymerizes to form a hardened aluminosilicate network. The process results in a cementitious material that can exhibit mechanical properties and durability similar to or in some cases exceeding OPC [4].

There has been promising signs related to environmental and mechanical performance. However, the application of AAMs is still limited due to challenges related to workability, setting behavior and variability in raw materials. One of the important parameters influencing these properties is the water glass modulus. This has an impact on the dissolution kinetics and also the rheological behavior of the system. Therefore there is an interest in understanding the relationship between activator modulus, rheological behavior, setting time and mechanical properties of the material to better optimize preparation of AAMs and implement them in

practical applications at a larger scale [2].

1.1 Aim

The overall aim of the project is to explore the use of sidestreams from steel manufacturing as a sustainable raw material used for concrete production. More specifically this project will investigate the alkali activator solution that dissolves the binder precursor and drive the formation of the binding gel in AAMs. The alkali activator modulus will be varied to see the impact it has on alkali-activated slag systems in relation to setting behavior, mechanical properties and microstructure. This project will also examine the impact of sustainable additives such as hemicellulose and lignin.

1.1.1 Specification of the Issue

- How does the water glass modulus affect reaction kinetics, microstructure, and compressive strength of alkali-activated blast furnace slag?
- What water glass modulus provides the best balance between setting time, microstructural development, and mechanical performance?
- Can lignin or hemicellulose be used as sustainable additives to improve mechanical or microstructural properties of alkali-activated blast furnace slag without excessively delaying setting time?

1.2 Scope

This work focuses on six different water glass solutions with varying water glass moduli. These alkaline activator solutions will be mixed with the same type of BFS. For this project a commercially available slag called Merit will be used. Sustainable additives, hemicellulose and lignin, will be added to some samples to investigate changes in setting time.

1.3 Limitations

This work is limited to one type of BFS, meaning the binder component is fixed and will not be the central point of investigation. Also the water-to-binder ratio is constant at 0.5 for all samples.

2
Theory

This chapter introduces the theoretical background relevant to alkali-activated slag systems. Key components, including BFS and sodium silicate activators are introduced, as well as reaction mechanisms, gel formation processes, and microstructural development governing the properties of the final material.

2.1 Alkali-Activated Slag Systems and Sustainable Binders

AAMs are a class of cementitious binders formed by aluminosilicate precursors reacting under alkaline conditions. The alkaline environment promotes the dissolution of reactive species from the binder precursor, primarily alumina and silica, which subsequently re-polymerizes to form a hardened binding gel.

Geopolymers are often considered a sub-category of AAMs and is typically referred to as low-calcium systems. These type of systems can be produced either through mixing with solely water or a two-part mix containing a liquid alkali activator [5]. In contrast, alkali-activated slags based on calcium-rich precursors, such as BFS, form different binding phases due to the high calcium content. BFS is a commonly used binder for alkali-activation. Slag systems that are derived from BFS or steel slags are characterized by a Ca/(Si+Al) ratio greater than one [6].

When BFS is used as a binder it requires quenching as well as grinding to a fine powder in order to obtain a reactive material. The amorphous structure formed during quenching enables dissolution under alkaline conditions. This leads to the ability for formation of calcium-(alumino)-silicate-hydrates (C-(A)-S-H) gels in the material [5].

Compared to OPC, AAMs are considered a more sustainable alternative given the lower CO_2 emissions and use of industrial by-products.

2.2 Blast Furnace Slag as a Binder

Waste materials from metallurgic processes are usually referred to as slag. BFS is a by-product of iron production formed during the smelting of iron ore in a blast furnace. Iron ore is reduced by coke, while limestone is added to remove impurities.

These impurities form a molten slag phase rich in calcium, silica and alumina, which is separated from iron and subsequently cooled to produce BFS.

BFS has been found to be one of the most useful waste material for cement and concrete manufacturing due to its chemical composition. It primarily consists of oxides that are typically also found in OPC. That includes CaO, SiO_2, Al_2O_3 and MgO [7]. These components make BFS a suitable binder for AAMs, as they provide the necessary reactive species for binder formation [7].

The cooling process of the slag strongly influences its properties. Rapid cooling of molten slag results in formation of a glassy, amorphous and granular material with low crystallinity [7]. This is typically done through water quenching. After water quenching granulated blast furnace slag (GBFS) is obtained [8]. The amorphous structure is highly reactive and therefore useful in applications of cementitious binders. Slow cooling leads to formation of crystalline phases, which reduces reactivity. As a result, rapid cooling is the preferred option for producing BFS as a binder for AAMs [9]. The granulated slag needs to be processed through drying and grinding into a fine powder, which is known as ground granulated blast furnace slag (GGBS) [10].

There is a commercially available GGBS called Merit. This slag is made from by-products in iron manufacturing. The manufacturer of Merit states that, per ton of produced cement, Merit emits 20-40 kg of CO_2, compared to conventional cement, which is responsible for 700-900 kg of CO_2 [11].

2.3 Water Glass and Alkali-Activator Solution

The alkali activator solution commonly consists of a sodium silicate solution, also known as water glass. One of the most important characteristics of water glass is the ability to form polymerized silicate gel networks that act as the binding phase in alkali-activated slag systems. The structure and distribution of silicate species is dependent on many factors such as solute concentration, silica-to-alkali ratio (water glass modulus), pH and temperature [12].

In AAMs, the binder material, contains silica, alumina and calcium oxide within an amorphous structure. Under alkaline conditions these species will dissolve and subsequently re-polymerize to form a binding gel [13]. Silicate species play an important role in controlling polymerization and gel network formation, aluminum adds cross-linking to the network through partial substitution of silicon to form Si-O-Al bonds, and calcium governs the formation of C-(A)-S-H gels, which are responsible for strength development of the material in Ca-rich systems [14].

It is possible to activate GGBS with a pure sodium hydroxide solution on its own, however the reactive species is limited to those released from the slag itself. This can restrict the extent of polymerization as well as the gel structure formed. The addition of water glass increases concentration of reactive species by addition of

dissolved silicate species to the system. It promotes formation of a more polymerized and well connected network and allows greater control of reaction kinetics [13].

The water glass modulus, which is defined as the SiO_2/Na_2O ratio, is what determines the balance between dissolved silicate species and alkalinity in the activating solution. This influences the dissolution kinetics, gel formation and the degree of polymerization within the system [15].

As mentioned previously, AAMs require alkali activation to form a material with excellent mechanical properties. Life cycle assessments comparing conventional concrete with AAMs has shown that fully or partially replacing Portland cement with alkali-activated slags significantly reduces environmental impact whilst still achieving the same compressive strength [16]. Water glass, which is a key component of AAMs has a significant energy demand when producing it. It is responsible for the largest carbon footprint contribution of AAMs. The cost of commercially available activator solutions is high when comparing AAMs to conventional cement based alternatives [16, 17].

2.4 Reaction Products and Network Polymerization

The main products formed from the reaction of BFS with an alkaline activator are C-(A)-S-H gels [18]. These gels differ to calcium-silicate-hydrate (C-S-H) gels formed in OPC systems, as they generally have a lower Ca/Si ratios but higher incorporation of aluminum. This results in a higher degree of polymerization. The C-(A)-S-H gels formed give rise to minerals that are called tobermorites. The secondary phases formed during curing is dependent on multiple factors such as alkalinity, water-to-binder ratio, curing environment, humidity and temperature [6].

Substitution of silicon by aluminum within the silicate network influences the structure and properties of the gel. Aluminum incorporation introduces negative charge imbalances in the framework, which must be compensated by cations such as Na^+ and Ca^{2+} [19]. This substitution increases cross-linking within the network and can alter the degree of polymerization, gel connectivity and microstructure of the material. As a consequence, the Si/Al ratio plays an important role in determining reaction kinetics, mechanical properties and durability of alkali-activated slag systems [20].

During the structural development of AAMs dissolved silica and alumina species polymerizes and forms new Si-O-Si and Si-O-Al bonds. These bonds are commonly grouped under the notation Si-O-T, where the "T" represents a tetrahedrally coordinated atom, typically silicon or aluminum. These reactions lead to formation of binding phases commonly referred to as gels. In Ca-rich systems, the primary binding gel is C-(A)-S-H [21].

The structure of these gels can be described in terms of Q^n silicate units. The n represents the number of bridging oxygen atoms surrounding the SiO_4 tetrahedron. The C-(A)-S-H gels are mainly composed of Q^1 and Q^2 units which corresponds to chain-like silicate structures. With increasing silicate content, the degree of polymerization increases, leading to a higher concentration of Q^3 units which are associated with cross-linking between the chains. These structural differences can be spotted in FTIR spectra as a shift of the Si-O-T main band to higher wavenumbers [5].

2.5 Microstructure and Porosity Development

AAMs formed from BFS undergo a heterogeneous reaction process involving several mechanisms. These include dissolution of the binder precursor particles, nucleation and growth of solid phases, interactions and bonding between reaction products, and diffusion-controlled reactions occurring through the formed reaction products during the later stages of curing. The primary reaction product formed in Ca-rich slag systems is an aluminum-substituted C-(A)-S-H type gel. The type of activator used has a strong influence on the C-(A)-S-H product and thus the final microstructure [21].

The microstructure and pore structure of alkali-activated binders play a critical role in determining their durability and mechanical performance. Pore development is strongly influenced by the alkalinity and pH of the activating solution, as these parameters affect dissolution kinetics, gel formation and the degree of polymerization within the system [21].

2.6 Setting Time and Mechanical Properties

Previous studies have shown that the water glass modulus can also strongly influence the setting time of AAMs. The fastest initial setting time (IST) has been reported at approximately water glass modulus 2.0, while both lower and higher modulus result in longer setting times [3].

The water glass modulus additionally affects the development of mechanical properties, as it influences dissolution kinetics, gel formation, and the degree of polymerization within the system. An optimal balance between alkalinity and dissolved silicate species is therefore important for achieving rapid setting and high compressive strength [21]. The water glass modulus has shown to greatly influence the viscosity of the solution. Research indicates there is a relationship between viscosity and the IST [3].

There are multiple standards available for cement that specify standardized test methods for relevant properties and define the requirements that different cement classes must fulfill [22, 23]. For setting time, SS-EN 196-3:2016 defines IST as "the time measured from zero at which the distance between the needle and the

base-plate is (6 ± 3) mm as the initial setting time of the cement to the nearest 5 min" [24].Since the sample depth according to the method is 40 mm, the IST corresponds to approximately 85% of the total penetration depth.

3
Methodology

This chapter focuses on describing the methods used for preparing the alkali-activator solutions, making the alkali-activated blast furnace slag, testing and characterization of the materials.

3.1 Raw Materials

This section includes a short description of the raw materials used for making the alkali activator solution as well as the binder material used.

3.1.1 Binder

For this project the commercially available GGBS called Merit (Swecem) was used, introduced in section 2.2. This slag is rich in Ca, Si, Mg and Al oxides. The notable compounds taking part in gel formation for AAMs are CaO, SiO_2, MgO and Al_2O_3. The composition of Merit is listed in Table 3.1 [11].

Table 3.1: Composition of Merit.

Compound	**Reference value**
CaO	34 %
SiO_2	36 %
MgO	13 %
Al_2O_3	13 %
FeO	0.38 %
MnO	0.41 %
TiO_2	1.8 %
Cl^-	0.0015 %
S^{2-}	0.26 %
SO_4	0.13 %
Na_2O	0.55 %
K_2O	0.70 %
Na_2O-ekvivalent	1.0 %

3.1.2 Alkali Activator Solution

The alkali activator solution was prepared with a sodium silicate solution (VWR) and a 50 % NaOH (Sigma-Aldrich) in water solution. The content of the sodium silicate solution was 25.6-27.6 % silicon dioxide and 7.5 - 8.5 % sodium oxide.

3.1.3 Lignin and Hemicellulose

Softwood Kraft lignin was received from Bäckhammar Pilot Plant (Bäckhammar, Sweden) where it was isolated with the LignoBoost method using industrial black liquor.

Hemicellulose (arabinoxylan) was extracted from wheat bran according to the method outlined by Börjesson et al. [25]

3.2 Preparation of Alkali Activator Solution

The project started with preparation of six alkali activator solutions with the following water glass moduli: 0.7, 1.0, 1.4, 1.7, 2.1, 2.5. The amount of water, sodium silicate solution and NaOH required to achieve a specific water glass modulus was calculated with a fixed solids content of 20 %. First water was added followed by sodium silicate and then a 50% NaOH solution. pH values and viscosity of the alkali activator solutions was measured as well.

3.3 Vicat Needle Test

An initial screening process was conducted to estimate the IST for each water glass modulus using the Vicat needle method. 50 g of Merit slag and 31.25 g of alkali activator solution were mixed to obtain a water-to-binder ratio of 0.5. The AAMs were prepared in paper cups to provide a larger surface area, allowing multiple needle penetrations at different locations during testing.

The test was performed by dropping the needle at set time stamps to track the penetration depth through the paste over time. A significant reduction of the penetration through the paste was taken as an indication that the AAM had past the IST. This test was repeated for all water glass moduli. If the sample had shown no drop in penetration depth within two hours the test was stopped. Duplicates was made for each water glass modulus.

When constructing graphs to present the results a linear interpolation of the duplicates was made to present an average curve for each water glass modulus. The IST value taken from each water glass modulus was at 85% of the total penetration depth.

3.4 Performance Tests of Alkali-Activated Slags

A compressive strength test was conducted for AAMs with water glass moduli 1.0, 1.4 and 2.1. The selected moduli were spread out to try and identify possible trends with compressive strength and modulus. The samples were prepared in molds to be tested after 7 and 28 days. The samples were prepared using the same water-to-binder ratio of 0.5 however these samples were also mixed with sand as aggregate. The aggregate-to-binder ratio was three. The sand that was used had a grain size particle distribution of 0-4 mm.

First the components were weighed separately. Alkal activator solution and GGBS was added first to the mixer followed by sand. After mixing the mortar was put into cubic shaped molds that were 4x4x4 cm in size. Three replicates was made for each composition. The mortars were left in the molds for three days to pass the IST. Then the cubic shaped blocks was removed from the molds and put in a climate room with set temperature at 20°C and a relative humidity of 50%. One of the prepared mortar samples can be seen in Figure 3.1

Figure 3.1: Cement mortar made in 4x4x4 cm mold

Compressive strength was tested with the Matest Cyber-Plus Progress that could measure concrete samples up to 300 kN. The instrument settings was the following: rate of 0.5 kN/s, start load of 0.1 kN, stop load of 10% and area of 1600 mm^2.

3.5 Microstructure and Chemical Characterization

This section describes the microstructural was analyzed as well as the chemical characterization of the AAMs.

3.5.1 Determination of Specific Surface Area

The alkali-activated samples were analyzed with a High Throughput Surface Area and Porosity Analyzer (TriStar3000, MicroMeritics) to determine their Brunauer-Emmett-Teller (BET) surface area. The samples from the Vicat tests were ground into fine powders. Prior to analysis, the samples were degassed with nitrogen gas at 60°C to remove physically adsorbed moisture. One sample failed the leak test under these conditions, meaning the measurement could not proceed. The degassing temperature at 60°C failed removing the moisture from some samples, which subsequently failed the leak test during analysis. Therefore degassing at 120°C was also tested successfully. Mild degassing temperatures were used to ensure the preservation of the microstructure of the materials and avoid pore collapse.

3.5.2 Fourier-Transform Infrared Spectroscopy

FTIR was performed to assess the chemical bonding in the alkali-activated samples. Finely ground powder of samples with water glass moduli 1.0, 1.4, 1.7 and 2.1 was used. The samples were analyzed at a wavelength from 4000 cm^{-1} to 400 cm^{-1}. The analysis was run at 4 resolutions with 64 accumulations. The obtained FTIR data was processed using Python and to construct a graph. A baseline correction was made by subtracting the average values from the 2500-3000 cm^{-1} region.

3.5.3 Scanning Electron Microscopy

SEM was conducted to investigate morphology and microstructure of the samples. The analysis was made for alkali-activated samples with water glass moduli 1.0, 1.4 and 1.7. Prior to analysis, the samples were embedded in epoxy resin to ensure stability during preparation. The embedded samples were then ground using silicon carbide abrasive papers of progressively finer grit sizes to obtain a flat and smooth surface suitable for imaging.

SEM imaging was carried out at an accelerating voltage of 15 kV at varying magnifications to obtain high-resolution microstructural images. Energy-dispersive X-ray spectroscopy (EDS) was conducted in conjuction with SEM to analyze elemental composition and spatial distribution of elements within the sample.

3.5.4 Thermogravimetric Analysis

Thermogravimetric analysis (TGA) was conducted to get an understanding of the AAMs major components. Samples with varying water glass moduli were crushed

and ground into fine powders. For each sample, 5-10 mg was weighed into small TGA crucibles, which were then placed in an autosampler. The analysis was carried out from 35°C to 900°C under an inert atmosphere with an N_2 flow of 60 ml/min. TGA was performed on moduli 1.0, 1.4, 1.7 and 2.1.

After the analysis, text files containing time, reference temperature, sample temperature, heat flow and weight were obtained. These data were used to construct graphs with normalized weight (%) as a function of temperature, as well as derivative thermogravimetric (DTG) curves.

3.5.5 Isothermal Calorimetry

Isothermal calorimetry analysis was conducted for water glass moduli 1.0, 1.4, 1.7 and 2.1. Duplicates were made for each modulus. The alkali-activated samples were prepared by mixing 12 g of GGBS with 7.5 g of alkali activator solution. The sample was then directly put into the calorimeter and the channel was switched on.

4

Results and Discussion

4.1 Screening of Setting Time

Figure 4.1 shows the normalized penetration depth through the cement paste as a function of time. The IST is shown by the clear drop of penetration depth. As can be seen from figure 4.1 the samples with water glass moduli 1.4, 1.7 and 2.1 has the earliest drop around 30-40 minutes indicating a fast IST. Samples with moduli 0.7 and 1.0 was slower and did not show a clear drop as observed with the faster samples. Modulus 2.5 did not show any change in penetration depth within 120 minutes. Based on this data water glass moduli 0.7 and 2.5 was not used for chemical characterization and performance tests.

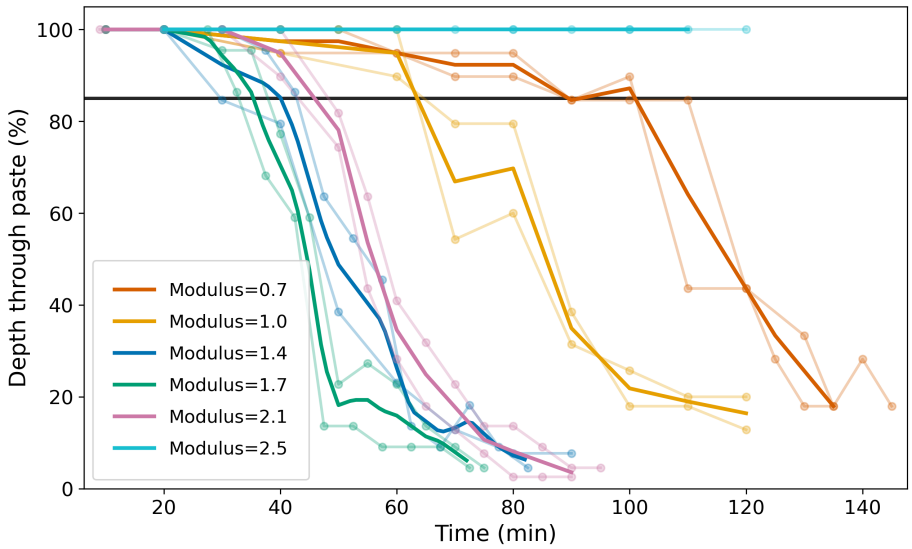

Figure 4.1: Vicat needle test measurement

To investigate the relationship between setting time and water glass modulus, the IST corresponding to 85% penetration depth was plotted against the water glass modulus, as shown in Figure 4.2a. The results show that setting time decreases rapidly with an increasing water glass modulus up to modulus 1.7, after which it starts to increase again for modulus 2.1. The data suggests there is an optimum modulus for minimizing setting time, however more data points with intermediate moduli would be needed to more accurately establish where the actual minimum is.

In Figure 4.2b, both pH and viscosity are plotted as a function of water glass modulus. A clear decrease in pH can be observed with an increasing SiO_2/Na_2O ratio, which is expected since higher modulus contains relatively lower amount of Na_2O and therefore exhibits lower alkalinity. Simultaneously, the silicate species become increasingly polymerized, resulting in changes to the solution structure and often an increase in viscosity.

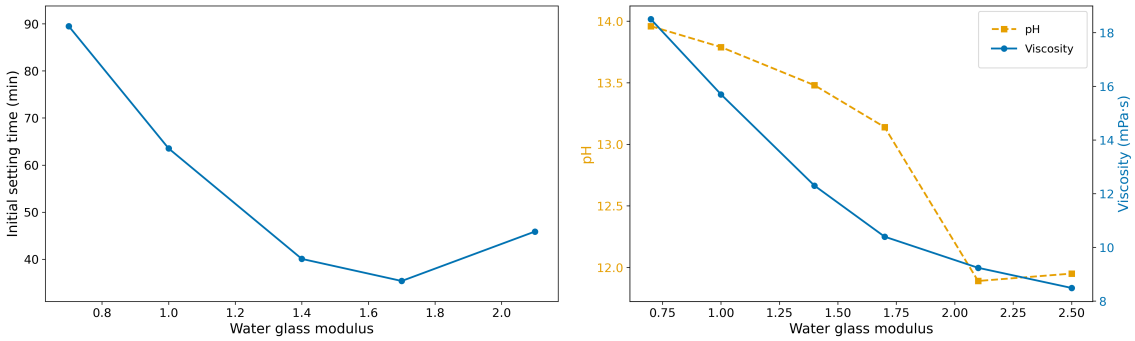

(a) Initial setting time as a function of modulus

(b) pH and viscosity as a function of modulus

Figure 4.2: Effect of water glass modulus on setting time, pH and viscosity in alkali activator solution

4.1.1 The Effect of Ligning and Hemicellulose

The Vicat needle tests results with sustainable additives is shown in Figure A.1. With 1% hemicellulose and lignin the samples did not show any sign of setting within two hours. The day after the sample had still not properly set and was still a soft paste. For 0.5% the samples showed a significant drop in penetration depth at 30-40 minutes. This is similar to the regular sample with water glass modulus 1.7. Therefore 0.5% is likely too low of a concentration to produce a clear effect. Further tests would need to be conducted to find the cut off point between 0.5 and 1.0%.

4.2 Isothermal Calorimetry

The isothermal calorimetry results are presented through four graphs. Figure 4.3a shows the full 24-hour heat evolution. This calorimetry curve shows typical behavior of alkali-activated systems, including a rapid dissolution peak followed by main reaction peak and a slower secondary heat evolution stage. The first exothermic peak can be assigned to dissolution of the binder precursor (mainly silica and alumina species). The second exothermic peak is assigned to the polymerization of the dissolved species and formation of C-(A)-S-H gels [26]. Figure 4.3b shows the heat evolution from 0-1.25 hours. Even though the same recipe was used for all samples the amplitude of the peaks differs quite significantly. This could be due to some uncertainties from the analysis. For example, the time for mixing differed between the samples and they were all mixed with a spoon by hand. This could

be a contributing factor to the irregular amplitude of the peaks. Therefore more emphasis was put on the position of the peaks.

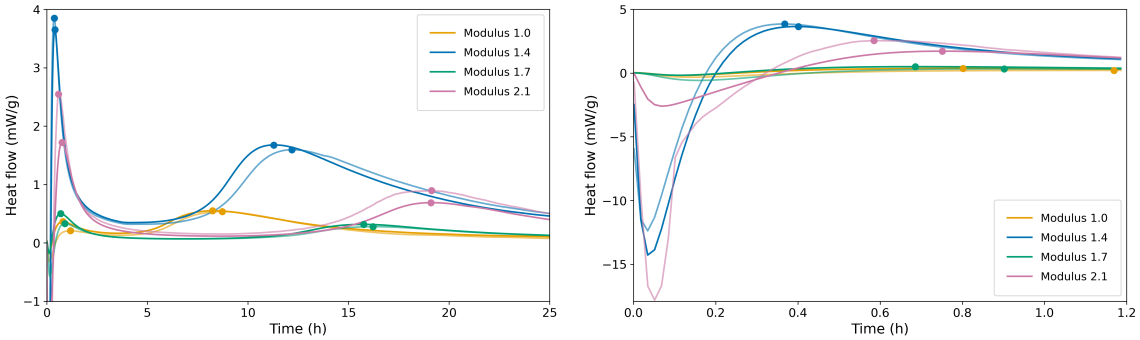

(a) Heat flow development over 25 hours **(b)** Magnified view of dissolution peak

Figure 4.3: Effect of water glass modulus on isothermal calorimetry behavior

The positions of the peaks shifted between the different moduli. However, there is no clear trend from the first peak. This can be seen from Figure 4.4a. The standard deviation is large for all moduli and no clear trend. However, from the second peak shown in Figure 4.4b a clear trend with a delayed second peak time with increasing water glass modulus can be observed. This suggests that lower alkalinity slows down formation of the main binding gels. Therefore a lower water glass modulus seems to be preferable for earlier structural development.

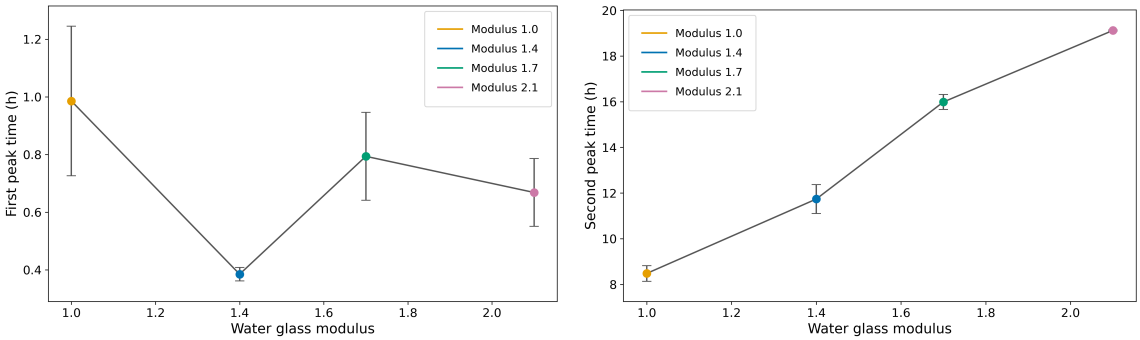

(a) Average first peak time for different water glass moduli (error bars represent standard deviation)

(b) Average second peak time for different water glass moduli (error bars represent standard deviation)

Figure 4.4: Influence of water glass modulus on calorimetric peak times

4.3 Molecular Structure

4.3.1 Phase Analysis

The TGA results could be used to identify the major components of the AAMs, as well as how they differ from raw Merit. Figure 4.5a shows the DTG graph of pure Merit without alkali activation and the other alkali-activated samples with different

moduli. It shows a clear difference between alkali activation and the precursor material. Which is a good indication that the wanted products has been formed. The downward peaks show the main events taking place up to 900°C. The first two peaks is associated with loss of freely bound water followed by dehydration of C-(A)-S-H gels. At 380°C there is hydrotalcite and the peak between 700-800°C is associated with calcium carbonate. Research has shown that decomposition of hydrotalcites occurs in three steps, where the third step is up to 400°C and involves the dehydroxylation and decarbonation of the hydrotalcite framework [27].

A shift of the peaks to higher temperature with increasing modulus can be noted, see Figure 4.5b. This is sign that higher silica content in relation to sodium leads to higher thermal stability. This is also supported by the broader region 300-600°C which is also consistent with higher modulus leading to a higher thermal stability. The rate of mass loss was calculated from the TGA results, available in Figure A.2.

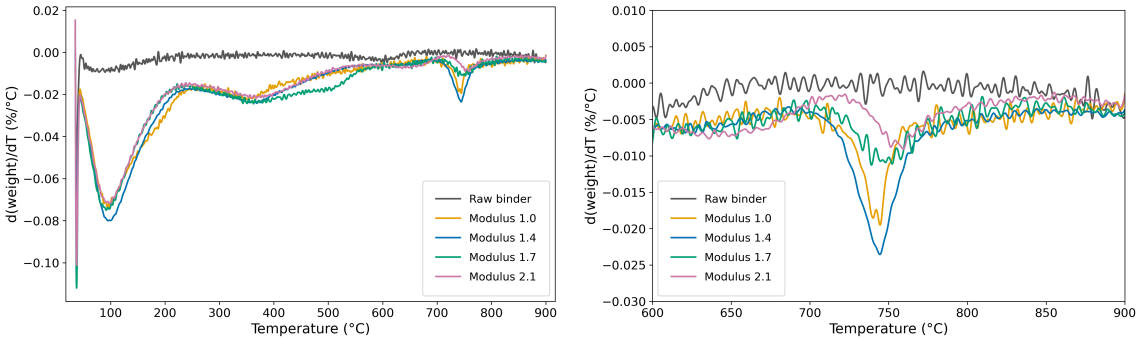

(a) Full DTG curve over the full temperature range

(b) Maginified view of calcite decomposition peak

Figure 4.5: Derivative thermogravimetric analysis

4.3.2 Chemical Bond Characterization

The FTIR spectra was used to characterize bonds in the alkali-activated slag system. Figure 4.6 shows the relevant downward band and peaks of raw binder material and four different alkali-activated samples. The broad band at 960 cm^{-1} is associated with vibrations of Si-O-T bond from Si-O_4 tetrahedrons [13]. This peak is common for all samples. The absorption band at 1650 cm^{-1} comes from H-O-H bending vibration [28]. The band from 1420 to 1500 cm^{-1} is associated with $CO_3{}^{2-}$ asymmetric stretching. When comparing the raw Merit band with alkali-activated samples there has been a shift of the band. This could be a result of a reorganization of the alumino-silicate network suggesting formation of C-(A)-S-H gels [29]. 875 is assigned to bending vibrations from $CO_3{}^{2-}$ in calcium carbonate [30, 31]. Table 4.1 summarizes the FTIR peak assignments.

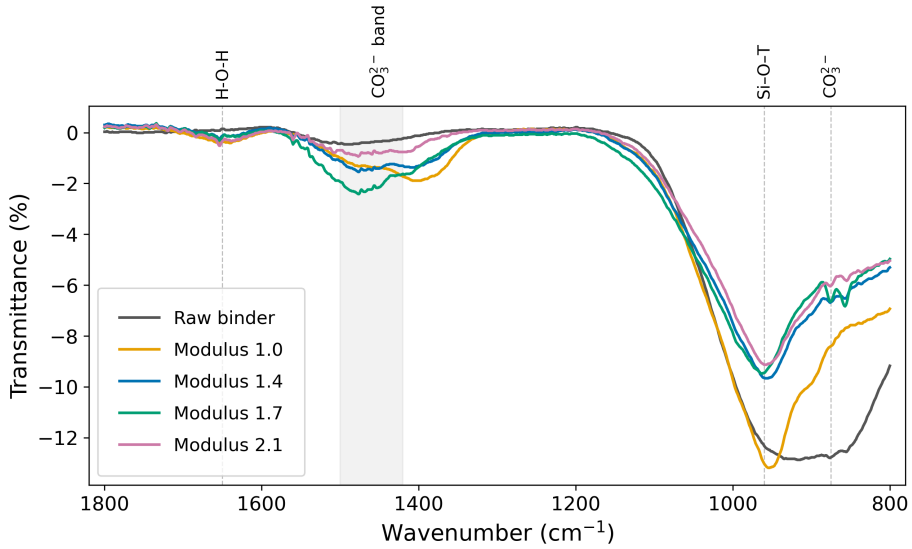

Figure 4.6: FTIR spectra

Table 4.1: Main FTIR peak assignments.

Wavenumber (cm^{-1})	**Assignment**	**Interpretation**
1650	H–O–H bending vibration	Physically bound / absorbed water
1450	CO_3^{2-} asymmetric stretching	Carbonation and calcite formation
960	Si–O–T asymmetric stretching	Aluminosilicate gel formation (T = Si or Al)
875	CO_3^{2-} bending vibration	Carbonate phases / calcite confirmation

Modulus 1.0 has a shifted peak to a higher wavenumber for the Si-O-T network at 960 cm^{-1}. This could be linked to the early structural development shown from the isothermal calorimetry results in Figure 4.4b. Meaning that modulus 1.0 has more restructuring of the network over time.

4.3.3 Elemental Mapping

This section summarizes results from SEM analysis on samples with water glass moduli 1.0, 1.4 and 1.7. Figure 4.7 shows a SEM image of modulus 1.4 at a scale of 80μm. The brighter larger particles is most likely unreacted slag particles from the binder material. Then the darker area surrounding the particles is the binding phase, which are C-(A)-S-H gels. SEM images of water glass moduli 1.0, 1.4 and 1.7 is shown in Figures A.3, A.4 and A.5 respectively.

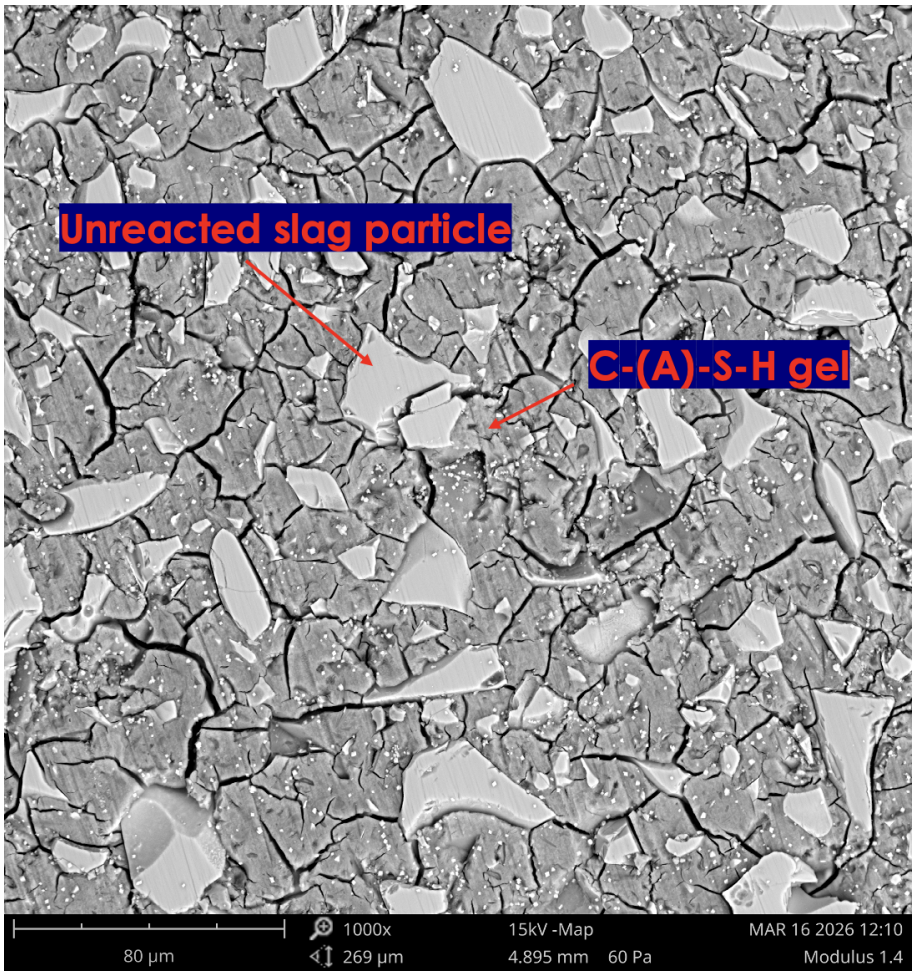

Figure 4.7: SEM image of AAS with water glass modulus 1.4

Table 4.2 shows the EDS elemental maps of the four main elements involved in the alkali-activated system. Elemental maps of additional elements is seen in Table A.1. Calcium and silicon is clearly present and uniformly distributed throughout the matrix. Aluminum also shows some presence in the matrix but not with the same intensity as calcium. This is consistent with aluminum substituting some of the silicon in C-(A)-S-H gels. Magnesium shows sign of forming localized secondary phase structures, which are visible as bright spots that are spatially distinct from the matrix. Many of the spots are not present in the aluminum and calcium maps.

Table 4.2: EDS elemental maps for different water glass moduli.

Water glass modulus	Al	Ca	Mg	Si
1.0	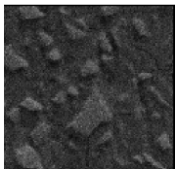	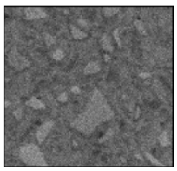	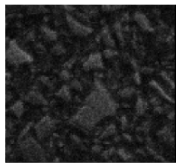	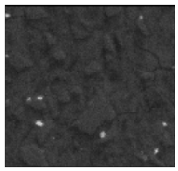
1.4	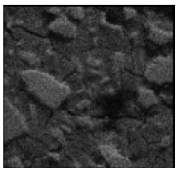	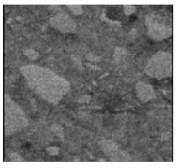	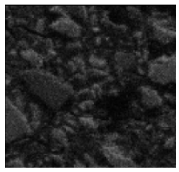	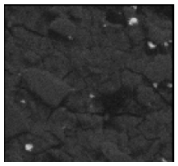
1.7	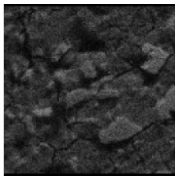	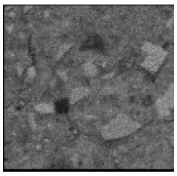	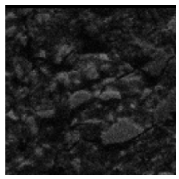	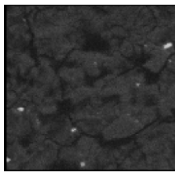

4.4 Microporosity and Surface Area

Surface area and porosity analysis showed a clear trend of increasing BET surface area with higher water glass modulus, as seen in Table 4.3. The same trend can be seen with total pore volume. Additional data from the surface area and porosity analysis can be seen in Table A.2

Table 4.3: BET surface area and total pore volume for alkali-activated materials with different water glass moduli.

Sample	Total pore volume (cm^3/g)	BET surface area (m^2/g)
Modulus 1.0	0.0154 ± 0.0013	4.3 ± 0.3
Modulus 1.4	0.0359	14.3
Modulus 1.7	0.0624	32.8

4.5 Compressive Strength

The results of compressive strength after 7 and 28 days show a dependence on the water glass modulus, as seen in Figure 4.8. For all mixtures the highest compressive strength is seen after 7 days, followed by a lower maximum strength after 28 days. Modulus 1.0 exhibited the highest compressive strength at both curing times, reaching approximately 46 MPa after 7 days and 36 MPa after 28 days. The lowest compressive strength was observed with modulus 2.1, with approximately

33 MPa after 7 days and 27 MPa after 28 days. The error bars in the graph represents the standard deviation of the replicate measurements and indicate a good reproducibility.

Based on the ratios that were tested, increasing the water glass modulus leads to a reduction at both 7 and 28 days. As lower water glass modulus exhibits higher compressive strength it indicates that higher alkalinity and promoting dissolution of the binder precursor and release of reactive silica and aluminum species leads to higher compressive strength. This is supported by the isothermal calorimetry results. Which indicated that increasing modulus resulted in slower formation of the main binding gel. It can also be linked back to the BET surface area results where higher modulus showed a higher porosity. Therefore showing a relationship between mechanical performance and porosity.

OPC does not typically show a trend of decreasing compressive strength over time as observed from these results. OPC shows an increasing compressive strength over time [32]. The reason behind this unexpected relationship could be down to sample preparation. The 7-day curing samples were prepared following the preparation of the 28-day samples and empirical knowledge contributed to improvement of the method. Thus, the 7-day samples were produced with better mixing practices leading to more homogeneous mixtures, less air entrapment and smoother surfaces. Another explanation could be that alkali-activated slags are more sensitive to drying shrinkage compared to OPC causing a higher degree of internal cracking. This aligns with the SEM results that showed internal cracking present in all alkali-activated samples, see Figure 4.7.

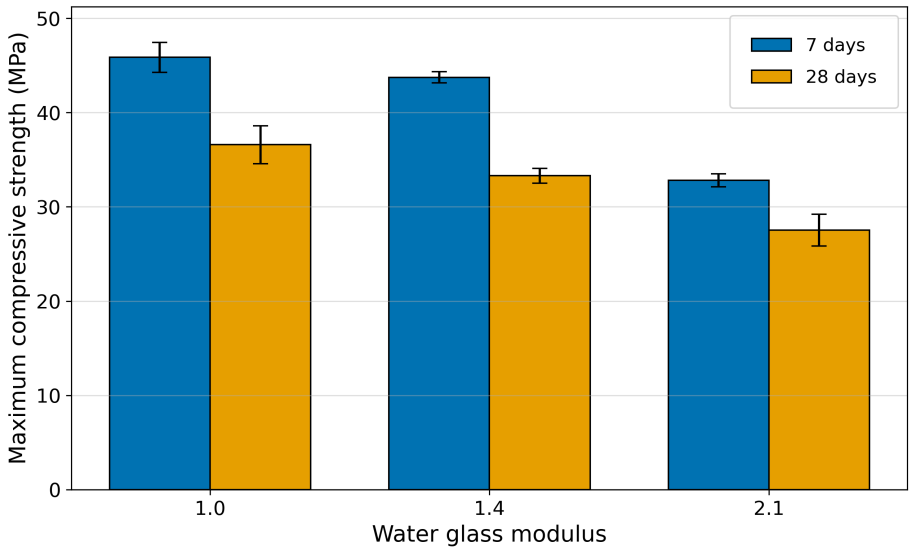

Figure 4.8: Compressive strength results (error bars represent standard deviation)

5

Conclusion

This study investigated how varying the water glass modulus influenced the setting behavior, microstructure and mechanical properties in alkali-activated BFS systems. The results strongly suggests that the modulus affects these parameters.

5.1 Main Findings

The Vicat needle tests showed a clear relationship between water glass modulus and IST. This is line with previous studies. The fastest IST was observed for modulus 1.7, while both lower and higher modulus values resulted in delayed setting. However, modulus 1.7 may not be practically desirable in cementitious systems due to the relatively short setting time compared to common standards for cement paste. Therefore a modulus of 1.0 or 2.1 with delayed IST based of the Vicat results should be more desirable.

Isothermal calorimetry further demonstrated how the water glass modulus influenced reaction kinetics and the structure development. A clear trend of delayed structure development with increasing modulus was observed.

FTIR analysis indicated structural differences between systems through changes in silicate-related bands associated with polymerization and gel formation. SEM/EDS observations further confirmed the heterogeneous microstructure typical of alkali-activated slag systems and supported the presence of C-(A)-S-H gels as the primary reaction product.

Combining BET surface area measurements with compressive strength results suggested a relationship between porosity and mechanical performance. Increasing modulus generally resulted higher surface area and porosity, while lower modulus systems exhibited denser structures and higher compressive strength. Modulus 1.0 showed a favorable balance between reaction kinetics, porosity and strength development.

Overall, the results demonstrate that the water glass modulus is a critical parameter in alkali-activated slag systems, as it governs reaction kinetics, microstructure development and mechanical performance. Optimizing the balance between alkalinity and dissolved silicate species is therefore essential for developing high-performance and more sustainable cementitious materials.

5.2 Limitations and Future Work

It is important to note that all systems were prepared using a fixed water-to-binder ratio of 0.5. The influence of varying this parameter was therefore not investigated and may significantly alter the results. Additionally, long-term durability was not investigated for this project.

Further studies should investigate the combined influence of water glass modulus and water-to-binder ratio. Additional long-term studies focusing on durability, shrinkage behavior and carbonation resistance would further improve understanding of alkali-activated slag systems.

5.3 Disclosure and Declaration of AI Use

AI-based tools were used to assist with generation of scripts for data processing and graphical representation of the experimental results.

Bibliography

[1] Mike Scott. *Cement: Building a green path in a hard industry*. June 2025. URL: https://www.reuters.com/sustainability/decarbonizing-industries/cement-hard-industry-crack-down-emissions-2025-06-11/.

[2] Laura Rossi et al. "Future perspectives for alkali-activated materials: from existing standards to structural applications". In: *RILEM Technical Letters* 7 (2022), pp. 159–177. ISSN: 25180231. DOI: 10.21809/rilemtechlett.2022.160.

[3] Helén Jansson, Diana Bernin, and Kerstin Ramser. "Silicate species of water glass and insights for alkali-activated green cement". In: *AIP Advances* 5.6 (June 2015). ISSN: 2158-3226. DOI: 10.1063/1.4923371. URL: https://doi.org/10.1063/1.4923371.

[4] Osama Ahmed Mohamed. "A Review of Durability and Strength Characteristics of Alkali-Activated Slag Concrete." In: *Materials (Basel, Switzerland)* 12.8 (Apr. 2019). ISSN: 1996-1944. DOI: 10.3390/ma12081198.

[5] John L. Provis. "Alkali-activated materials". In: *Cement and Concrete Research* 114 (Dec. 2018), pp. 40–48. ISSN: 00088846. DOI: 10.1016/j.cemconres.2017.02.009.

[6] Markssuel Teixeira Marvila, Afonso Rangel Garcez de Azevedo, and Carlos Maurício Fontes Vieira. *Reaction mechanisms of alkali-activated materials*. 2021. DOI: 10.1590/s1983-41952021000300009.

[7] Bob Talling and Pavel Krivenko. "Blast furnace slag-the ultimate binder". In: *Waste Materials Used in Concrete Manufacturing*. Elsevier, 1996, pp. 235–289. DOI: 10.1016/B978-081551393-3.50008-9.

[8] Mehrab Nodehi, Togay Ozbakkaloglu, and Aliakbar Gholampour. "Effect of supplementary cementitious materials on properties of 3D printed conventional and alkali-activated concrete: A review". In: *Automation in Construction* 138 (June 2022), p. 104215. ISSN: 09265805. DOI: 10.1016/j.autcon.2022.104215.

[9] F. Engström et al. "Crystallization Behaviour of some Steelmaking Slags". In: *steel research international* 81.5 (May 2010), pp. 362–371. ISSN: 1611-3683. DOI: 10.1002/srin.200900154.

[10] Maebh A. Grace, Eoghan Clifford, and Mark G. Healy. "The potential for the use of waste products from a variety of sectors in water treatment processes". In: *Journal of Cleaner Production* 137 (Nov. 2016), pp. 788–802. ISSN: 09596526. DOI: 10.1016/j.jclepro.2016.07.113.

[11] Swecem. *Merit*. URL: https://swecem.se/merit/.

[12] Marzieh Matinfar and John A. Nychka. "A review of sodium silicate solutions: Structure, gelation, and syneresis". In: *Advances in Colloid and Interface Science* 322 (Dec. 2023), p. 103036. ISSN: 00018686. DOI: 10.1016/j.cis.2023.103036.

[13] F. Puertas et al. "A model for the C-A-S-H gel formed in alkali-activated slag cements". In: *Journal of the European Ceramic Society* 31.12 (Oct. 2011), pp. 2043–2056. ISSN: 09552219. DOI: 10.1016/j.jeurceramsoc.2011.04.036.

[14] O. Mikhailova et al. "In situ characterization of main reaction products in alkali-activated slag materials by Confocal Raman Microscopy". In: *Cement and Concrete Composites* 99 (May 2019), pp. 32–39. ISSN: 09589465. DOI: 10.1016/j.cemconcomp.2019.02.004.

[15] Jianwei Sun and Zhonghui Chen. "Effect of silicate modulus of water glass on the hydration of alkali-activated converter steel slag". In: *Journal of Thermal Analysis and Calorimetry* 138.1 (Oct. 2019), pp. 47–56. ISSN: 1388-6150. DOI: 10.1007/s10973-019-08146-3.

[16] Mohan Jiang et al. "Comparative Life Cycle Assessment of Conventional, Glass Powder, and Alkali-Activated Slag Concrete and Mortar". In: *Journal of Infrastructure Systems* 20.4 (Dec. 2014). ISSN: 1076-0342. DOI: 10.1061/(ASCE)IS.1943-555X.0000211.

[17] Katja König et al. "Evaluation of locally available amorphous waste materials as a source for alternative alkali activators". In: *Ceramics International* 47.4 (Feb. 2021), pp. 4864–4873. ISSN: 02728842. DOI: 10.1016/j.ceramint.2020.10.059.

[18] Chao Li et al. "C-A-S-H Gel and Pore Structure Characteristics of Alkali-Activated Red Mud–Iron Tailings Cementitious Mortar". In: *Materials* 15.1 (Dec. 2021), p. 112. ISSN: 1996-1944. DOI: 10.3390/ma15010112.

[19] P. Faucon et al. "Aluminum Incorporation in Calcium Silicate Hydrates (CSH) Depending on Their Ca/Si Ratio". In: *The Journal of Physical Chemistry B* 103.37 (Sept. 1999), pp. 7796–7802. ISSN: 1520-6106. DOI: 10.1021/jp990609q.

[20] Ewa Kapeluszna et al. "Incorporation of Al in C-A-S-H gels with various Ca/Si and Al/Si ratio: Microstructural and structural characteristics with DTA/TG, XRD, FTIR and TEM analysis". In: *Construction and Building Materials* 155 (Nov. 2017), pp. 643–653. ISSN: 09500618. DOI: 10.1016/j.conbuildmat.2017.08.091.

[21] John L Provis and Jannie S J Van Deventer. *RILEM State-of-the-Art Reports State-of-the-Art Report, RILEM TC 224-AAM*. Tech. rep. URL: http://www.springer.com/series/8780.

[22] ASTM International. *Test Methods for Time of Setting of Hydraulic Cement by Vicat Needle*. West Conshohocken, PA, Oct. 2021. DOI: 10.1520/C0191-21. URL: http://www.astm.org/cgi-bin/resolver.cgi?C191-21.

[23] Swedish Institute for Standards (SIS). *SVENSK STANDARD Cement-Del 1: Sammansättning och fordringar för ordinära cement Cement-Part 1: Composition, specifications and conformity criteria for common cements*. Tech. rep. 2011. URL: www.sis.se.

[24] Swedish Institute for Standards (SIS). *SVENSK STANDARD Cement-Provning-Del 3: Bestämning av bindetid och volymbeständighet Methods of testing cement-Part 3: Determination of setting times and soundness*. Tech. rep. 2016. URL: www.sis.se.

[25] Mikaela Börjesson et al. "Thermoplastic and Flexible Films from Arabinoxylan". In: *ACS Applied Polymer Materials* 1.6 (June 2019), pp. 1443–1450. ISSN: 2637-6105. DOI: 10.1021/acsapm.9b00205.

[26] Zuhua Zhang et al. "Quantitative kinetic and structural analysis of geopolymers. Part 2. Thermodynamics of sodium silicate activation of metakaolin". In: *Thermochimica Acta* 565 (Aug. 2013), pp. 163–171. ISSN: 00406031. DOI: 10.1016/j.tca.2013.01.040.

[27] Sara J. Palmer, H. J. Spratt, and R. L. Frost. "Thermal decomposition of hydrotalcites with variable cationic ratios". In: *Journal of Thermal Analysis and Calorimetry* 95.1 (Jan. 2009), pp. 123–129. ISSN: 1388-6150. DOI: 10.1007/s10973-008-8992-4.

[28] Claudio Finocchiaro et al. "FT-IR study of early stages of alkali activated materials based on pyroclastic deposits (Mt. Etna, Sicily, Italy) using two different alkaline solutions". In: *Construction and Building Materials* 262 (Nov. 2020), p. 120095. ISSN: 09500618. DOI: 10.1016/j.conbuildmat.2020.120095.

[29] Seifollah Nasrazadani et al. *Application of FTIR for Quantification of Alkali in Cement*. Tech. rep. 2011.

[30] Rikard Ylmén and Ulf Jäglid. "Carbonation of Portland Cement Studied by Diffuse Reflection Fourier Transform Infrared Spectroscopy". In: *International Journal of Concrete Structures and Materials* 7.2 (June 2013), pp. 119–125. ISSN: 1976-0485. DOI: 10.1007/s40069-013-0039-y.

[31] I. García Lodeiro et al. "Effect of alkalis on fresh C–S–H gels. FTIR analysis". In: *Cement and Concrete Research* 39.3 (Mar. 2009), pp. 147–153. ISSN: 00088846. DOI: 10.1016/j.cemconres.2009.01.003.

[32] Binna Lee, Jong Suk Lee, and Jae Suk Ryou. "Long-term Compressive Strength Properties of Concrete Incorporating Admixtures: Outdoor Exposure Testing in a Coastal Environment". In: *International Journal of Concrete Structures and Materials* 18.1 (Dec. 2024). ISSN: 22341315. DOI: 10.1186/s40069-024-00687-8.

A

Additional Graphs and Results

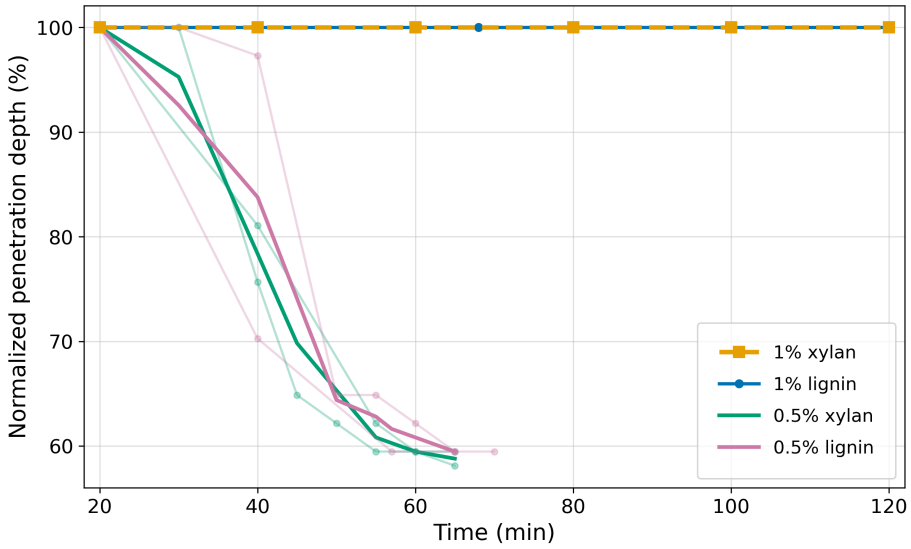

Figure A.1: Vicat results for alkali-activated samples with sustainable additives

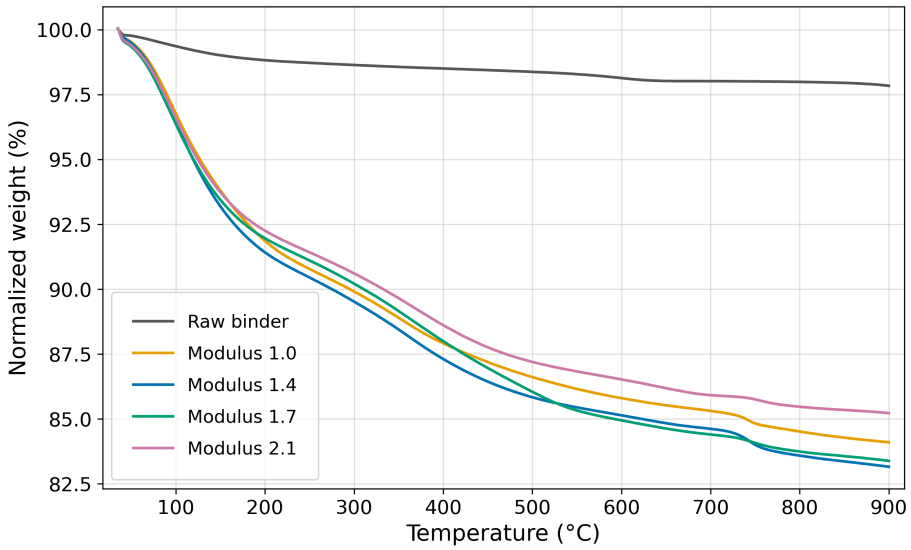

Figure A.2: TGA graph of raw binder and alkali-activated samples

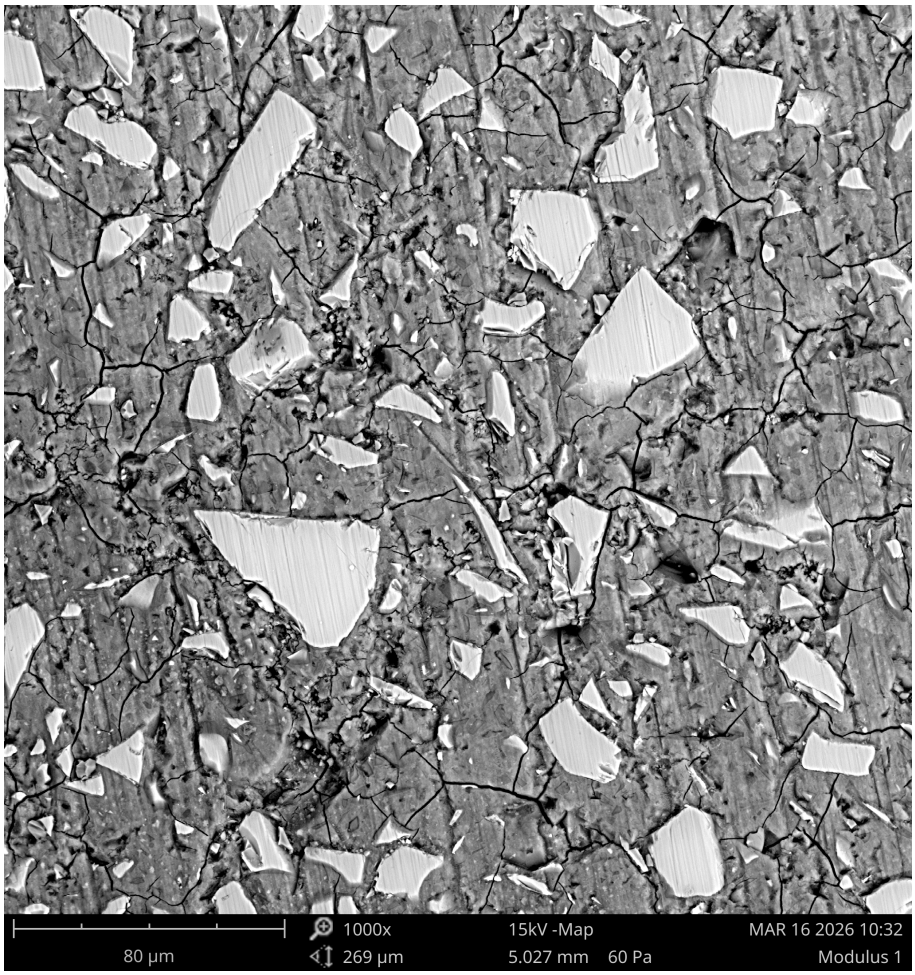

Figure A.3: SEM image of modulus 1.0

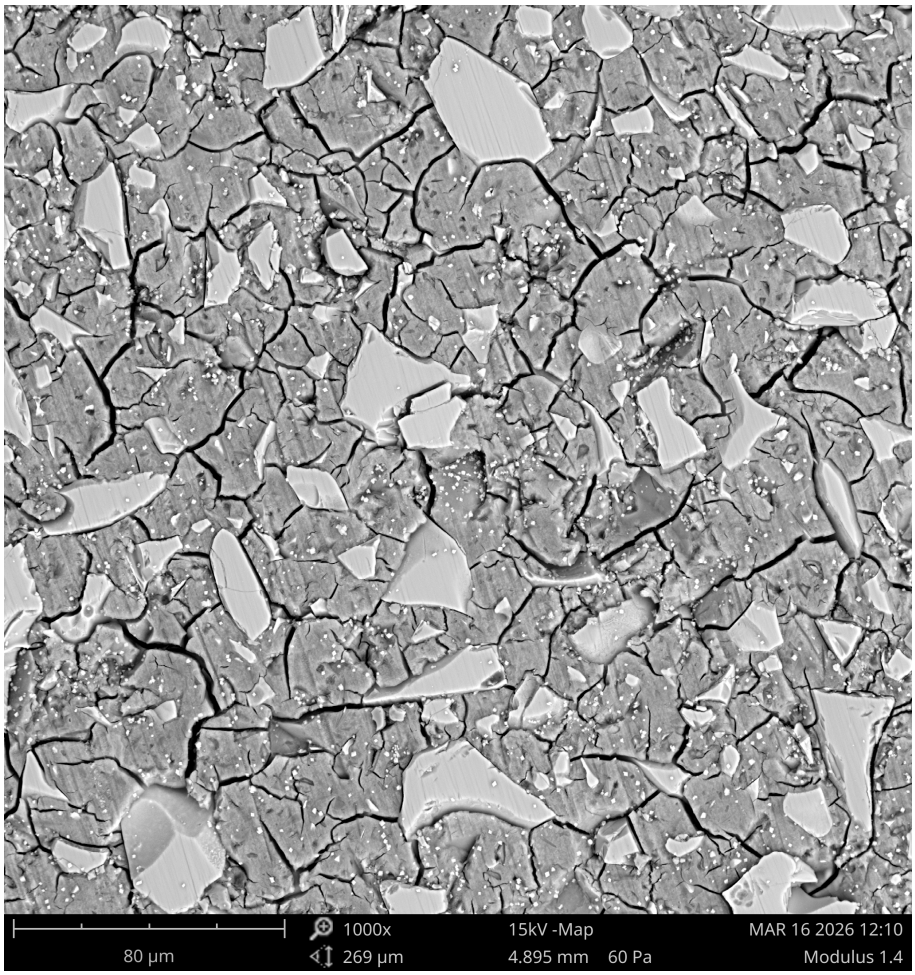

Figure A.4: SEM Image Modulus 1.4

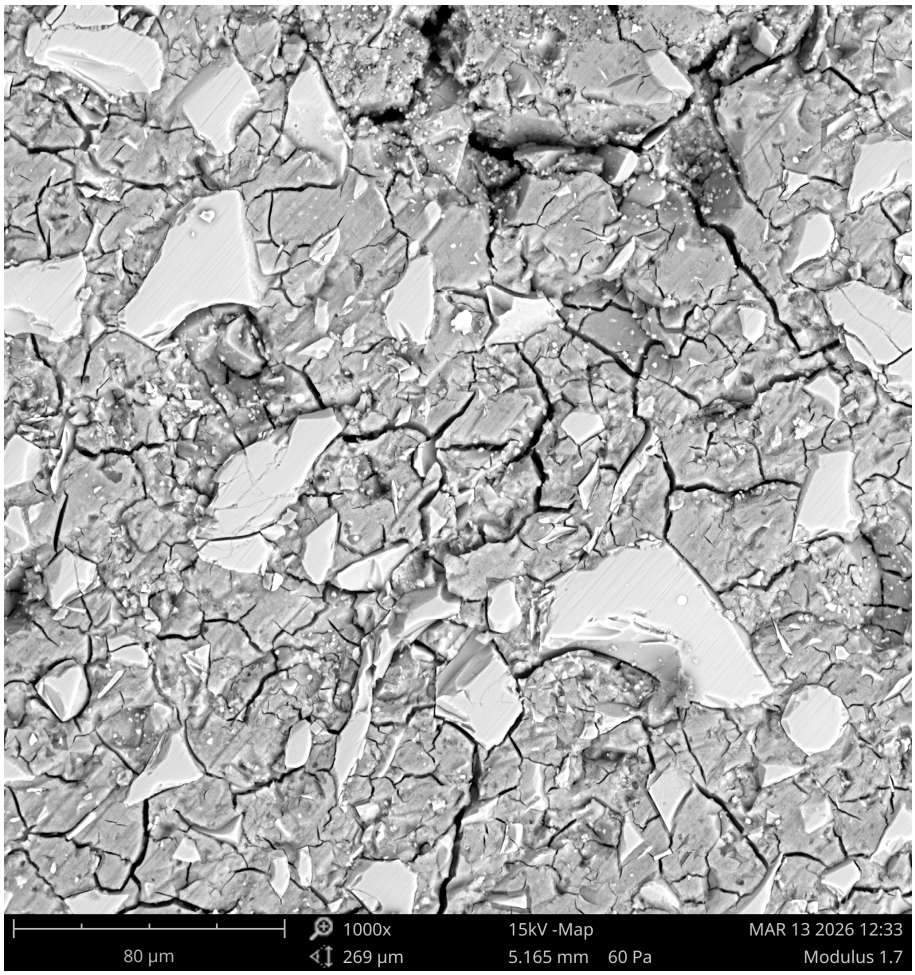

Figure A.5: SEM Image of Modulus 1.7

Table A.1: Elemental Maps for Different Water Glass Moduli.

Water glass modulus	O	Na	S	Ti
1.0	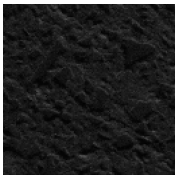	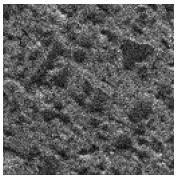	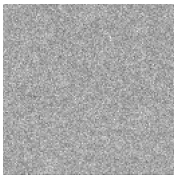	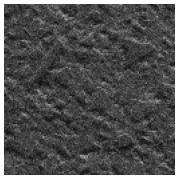
1.4	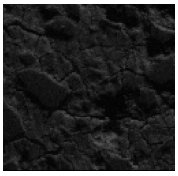	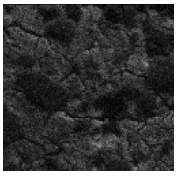	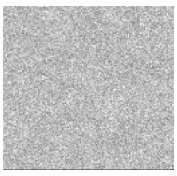	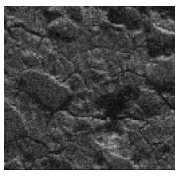
1.7	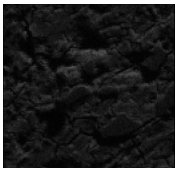	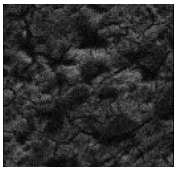	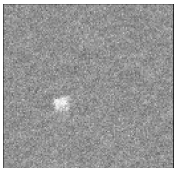	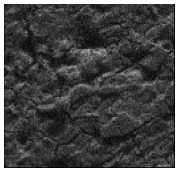

Table A.2: BET surface area, total pore volume, and pore size distribution for alkali-activated materials with different water glass moduli. F indicates finely ground material, C indicates coarse ground material, followed by the degassing temperature.

Sample	Total pore volume (cm^3/g)	BET surface area (m^2/g)	Pore size distribution (nm)
Modulus 1.0 F (60°C)	0.01400	4.1554	11.1–11.7
Modulus 1.0 F (120°C)	0.01546	4.0994	10.4–11.1
Modulus 1.0 C (120°C)	0.01666	4.5923	8.7–9.5
Modulus 1.4 (120°C)	0.03594	14.2709	8.1–8.9
Modulus 1.7 (150°C)	0.062383	32.8331	7.8

DEPARTMENT OF SOME SUBJECT OR TECHNOLOGY
CHALMERS UNIVERSITY OF TECHNOLOGY
Gothenburg, Sweden
www.chalmers.se

CHALMERS
UNIVERSITY OF TECHNOLOGY